Supplement of The Cryosphere, 17, 3505–3533, 2023
https://doi.org/10.5194/tc-17-3505-2023-supplement

The Cryosphere Open Access EGU

Supplement of

Investigating the thermal state of permafrost with Bayesian inverse modeling of heat transfer

Brian Groenke et al.

Correspondence to: Brian Groenke (brian.groenke@awi.de)

S1 Sensitivity of inversion method to available sensor depths

S1.1 Samoylov inversion without deep borehole temperature measurements

In order to investigate the impact of available borehole sensor depths on our inversion method, we ran an additional set of simulations for the Samoylov site with the measurements below $10\,\mathrm{m}$ omitted from the inference procedure. It is clear that omitting the deeper borehole observations for Samoylov primarily impacts the variability of the temperature profile at the beginning of the simulation period (Fig. S1). There appears to be little to no impact on the apparent relationship between long-term trends in temperature and latent heat/active layer thickness (Fig. S2), with the linear relationship between latent heat and temperature staying the same within the bootstrap margin of error: $(2.1 \pm 0.9)\,\mathrm{MJ/K}$ with all sensors depths to $(2.2 \pm 0.3)\,\mathrm{MJ/K}$ excluding depths below $10\,\mathrm{m}$. The change in the linear relationship between active layer thickness and temperature was also negligible: $(0.011 \pm 0.007)\,\mathrm{m/K}$ to $(0.014 \pm 0.002)\,\mathrm{m/K}$.

S1.2 Synthetic sensitivity analysis

To further elucidate the impact of available measurement depths on both cold and warm sites, we carried out additional inverse modeling experiments using synthetic pseudo-observations. We generated these pseudo-observations by first selecting the highest probability ensemble member (the posterior mode) from the ensemble results presented in Sec. 4.2 of the main text for both the Samoylov Island and Bayelva sites. We then took the mean annual ground temperatures computed from these two simulations and added zero-centered, Gaussian noise with scale decreasing exponentially as a function of depth, i.e:

$$\sigma(z) = 0.1 + (\sigma_0 - 0.1)\exp(-z/d) \tag{1}$$

where $\sigma_0 = 0.6$ is the maximum noise scale at $z = 0\,\mathrm{m}$ and $d = 5\,\mathrm{m}$ is the characteristic depth that determines the decay rate of the noise scale. We choose $d = 5\,\mathrm{m}$ since we can generally expect variation due to intraannual fluctuations to be minimal below this depth. We then run EKS three times for both site configurations using this synthetic data as the observations: first using only "shallow" temperatures ($2\,\mathrm{m}$ to $10\,\mathrm{m}$ with $1\,\mathrm{m}$ spacing), second using only "deep" temperatures ($20\,\mathrm{m}$ to $30\,\mathrm{m}$ with $2\,\mathrm{m}$ spacing) and finally using the full depth range (both shallow and deep in addition to depths $12\,\mathrm{m}$ to $20\,\mathrm{m}$ with $2\,\mathrm{m}$ spacing). For these experiments, we used a smaller ensemble size, $N = 128$, to reduce the computational requirements of the analysis. It is important to note that these experiments are only intended to investigate the sensitivity of the inversion algorithm to available sensor depths and do not necessarily demonstrate realistic conditions as they are constrained only by pseudo-observations.

The results of the depth sensitivity analysis shown in Figs. S3-S5 are, for the most part, fairly unsurprising. The accuracy of the predicted temperatures naturally improve when observations at or near this depth are included. For example, the modeled temperatures at $10\,\mathrm{m}$ depth show the most agreement with the synthetic observations in the "shallow" and "all" cases where observations are available near this depth (FIg. S3). In the "deep" case for both Samoylov and Bayelva, the model ensemble overestimates warming in the upper $10\,\mathrm{m}$ due to the lack of observations to constrain this part of the temperature profile. Similarly, we can see in Fig. S4 that the model ensemble underestimates warming at deeper depths in the "shallow" case due to the lack of observations below $10\,\mathrm{m}$. It is also clear that the availability of deeper measurements has a predictably large impact on the range of predicted initial temperature profiles at the beginning of the simulation period, as was also observed in Fig. S1. Note that these results, particularly the overestimated near-surface warming in the "deep" case (Fig. S3) has some implications for the results presented in the main text; i.e. it may be the case that our inversion for the Barrow site is actually overestimating temperature trends in the upper $10\,\mathrm{m}$ of the soil column due to the lack of observations available at these depths. This does not affect the main result of the study, however, which is not the absolute value of the modeled permafrost warming trends but rather their relationship with changes in latent heat.

The long-term energy change plots shown in Fig. S5 are also fairly predictable for the cold permafrost case at Samoylov and are consistent with the results presented in Sec. S1.1. Removing the deeper "measurements" below $10\,\mathrm{m}$ increases the overall spread of predicted sensible heat change, which is simply proportional to the changes in temperature seen in Figs. S3 and S4. What is more suprising, however, is the apparent increase in variability for the predicted latent heat storage in the peramfrost and active layers at Bayelva when "all" depths (from $2\,\mathrm{m}$ to $30\,\mathrm{m}$) are available. We might expect that including more observations at deeper depths in addition to observations in the upper $10\,\mathrm{m}$ would decrease our uncertainty about the

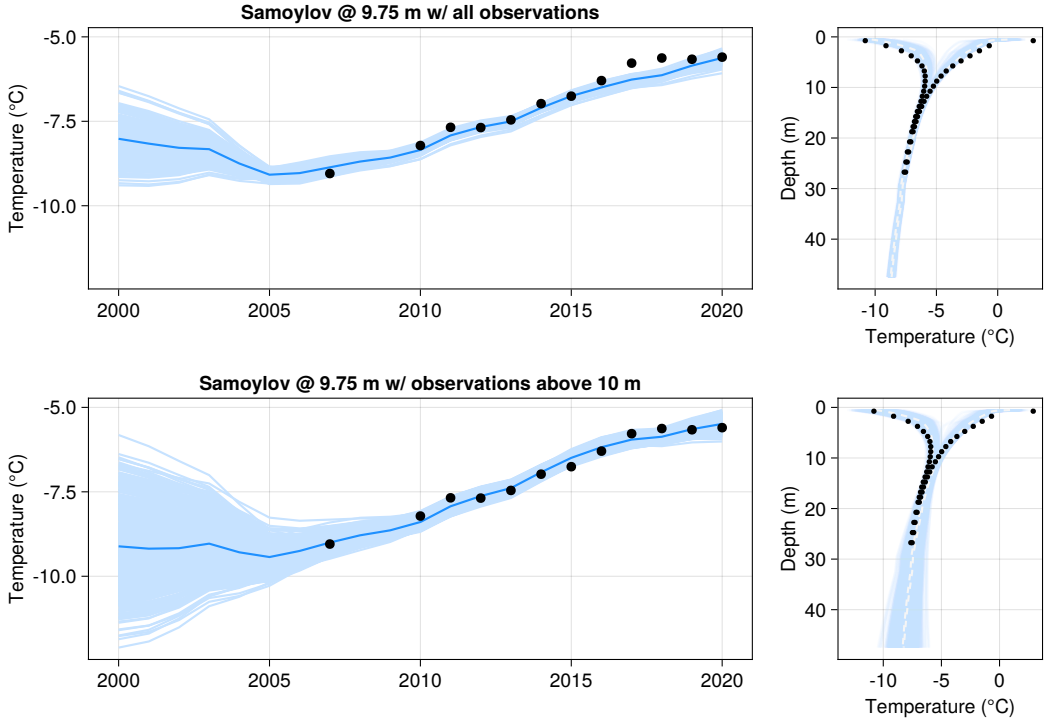

Figure S1. Mean annual ground temperatures at $9.75\,\mathrm{m}$ depth (the deepest sensor after truncation) at Samoylov along with temperature profiles in the final simulation year (2020) for all ensemble members. The dark blue line shows the ensemble mean. The dotted white line on the temperature profile plots shows the ensemble median. Note the recent change in the long-term warming trend at this depth within the last five years cannot be resolved by our current model due to the bidecadal n-factor parameterization. This change appears to not be due to air temperature but rather changes in snow cover, in particular substantial early-season snowfall in the winter of 2016/2017 (Boike et al., 2019).

overall thermal state of the system. However, as discussed extensively in the main text, the relationship between temperature and latent heat is not so straightforward. Higher porosity, for example, implies a larger volume of soil ice/water which results in more energy stored as latent heat. The parameter sensitivity plots shown in Sec. S2.2 show very clearly that latent heat trends are most sensitive to parameters relating to the forcing (i.e. n-factors), saturation level, freeze curves, and ground ice (porosity and excess ice), as well as the effective melting point, T_m. The most likely values of these parameters (i.e. those that produce temperatures which are most in agreement with observations) may result in higher uncertainty about latent heat due to their nonlinear relationship with temperature.

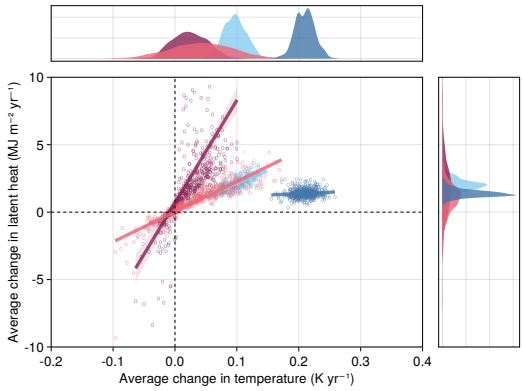

(a) Latent heat, all available measurements

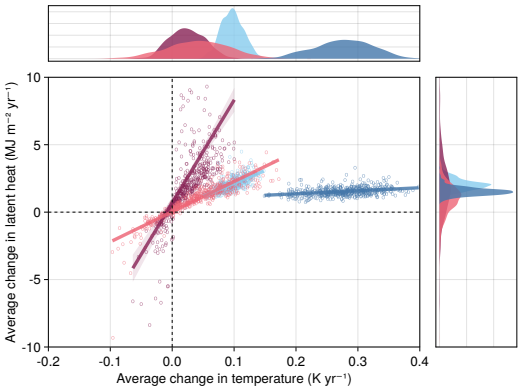

(b) Latent heat, measurements down to 10 m

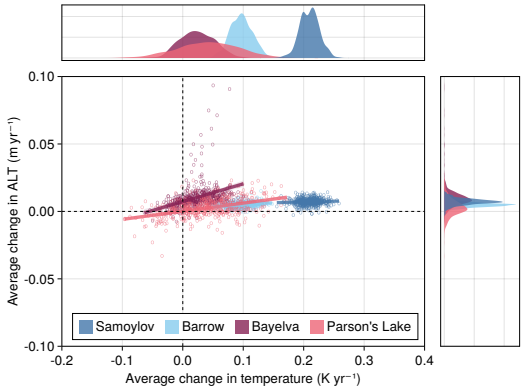

(c) Active layer thickness, all available measurements

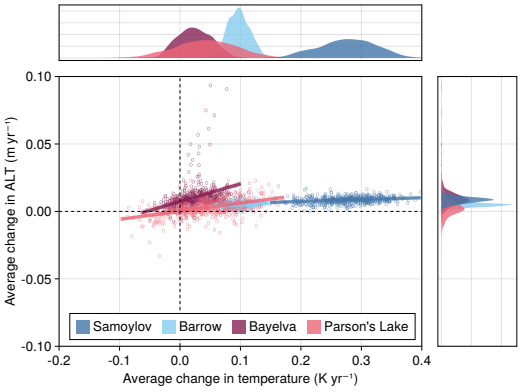

(d) Active layer thickness, measurements down to 10 m

Figure S2. Joint densities of modeled mean annual change in latent heat (a-b) and active layer thickness (c-d) vs. mean annual change in ground temperature across sites for both the normal Samoylov run with all borehole depths (a,c) and the additional Samoylov run with only borehole observations up to 10 m (b,d). Note that omitting the deeper sensors largely only affects the spread of observed temperature trends and not the relationship with changes in latent heat. In all four plots, a small number of points from Bayelva exceed the upper y-axis limit and thus are not shown.

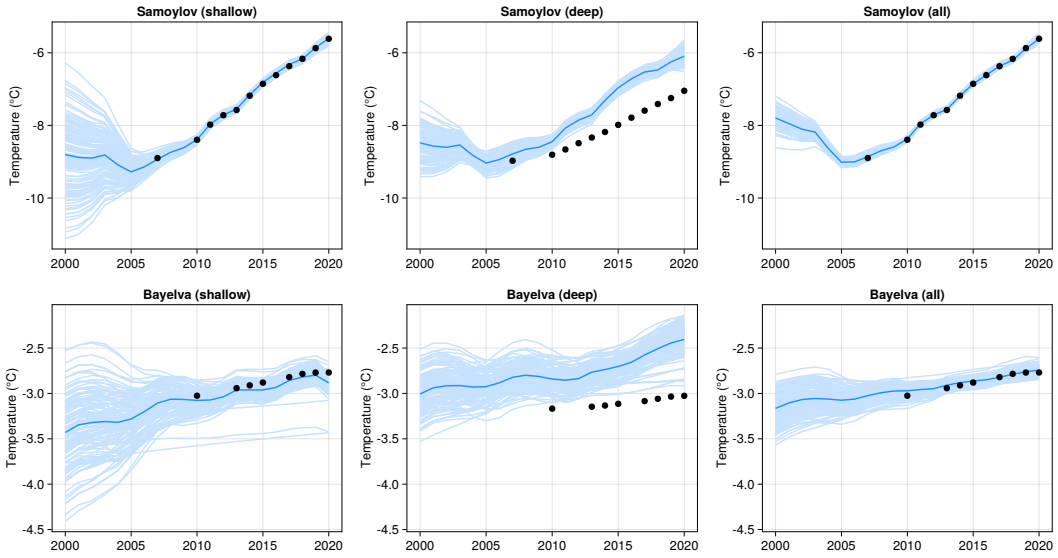

Figure S3. Mean annual ground temperatures at 10 m depth for all ensemble members and all three pseudo-observation depth cases: Shallow (2 m to 10 m), Deep (20 m to 30 m), and All (2 m to 30 m). The solid blue line is the ensemble mean. Black dots are the pseudo-observations used for fitting the ensemble with EKS.

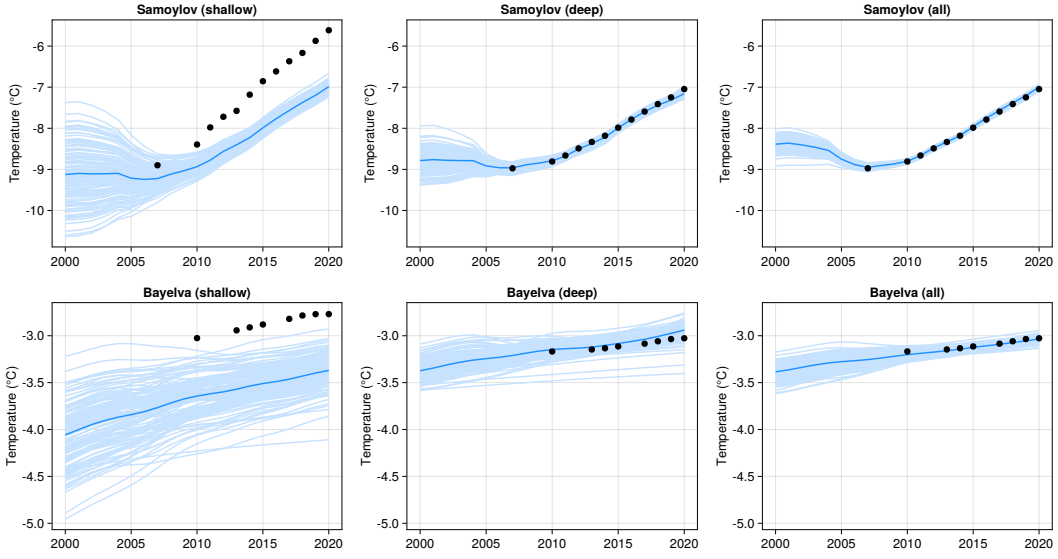

Figure S4. Mean annual ground temperatures at 20 m depth for all ensemble members and all three sensitivity cases: Shallow (2 m to 10 m), Deep (20 m to 30 m), and All (2 m to 30 m). The solid blue line is the ensemble mean. Black dots are the pseudo-observations (posterior mode predictions with additive noise) used for fitting the ensemble with EKS.

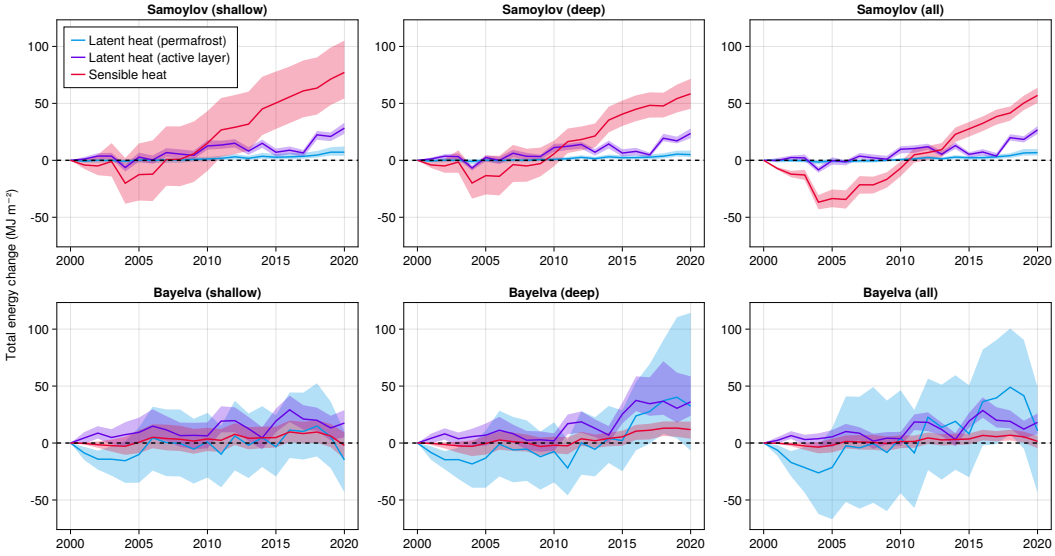

Figure S5. Total change in energy partitions (upper 10 m of soil profile) since the beginning of simulation period for each sensitivity case: Shallow (2 m to 10 m), Deep (20 m to 30 m), and All (2 m to 30 m). Energy is partitioned into three categories: Latent heat in frozen grid cells (i.e. cells with maximum annual temperature $T_{\max} < 0\,°\mathrm{C}$), latent heat in the active layer ($T_{\max} \geq 0\,°\mathrm{C}$), and sensible heat. Solid lines show the median energy change while the shaded regions show the 95% CCI over the ensemble.

S2 Model parameters

S2.1 Prior distributions

Tables S2 to S5 detail the prior distributions used for each parameter varied in the inversion procedure. We emphasize that these stratigraphy values are generally designed to be coarse estimates based on previous studies, field knowledge, and known characteristics of the landscape; uncertainty in the exact values is accounted for through the corresponding prior distributions, which allow for a modest amount of deviation (generally 10–20%) from the mean. Parameter names are summarized in Table A1 in the appendix of the main text which is reproduced here as Table S1.

Table S1. Names and descriptions of parameters considered in the ensemble inversion procedure. Some parameters appear multiple times across years or layers as indicated.

Identifier	Units	Description
`nfw@initial`	-	Initial wintertime n-factor used during spin-up period.
`nfw@[yyyy]`	-	Wintertime n-factor piecewise linear knot at year `yyyy`.
`nfs@initial`	-	Initial summertime n-factor used during spin-up period.
`nfs@[yyyy]`	-	Summertime n-factor piecewise linear knot at year `yyyy`.
`T0@active_layer`	°C	Upper-most knot in initial temperature profile within the active layer.
`T0@zaa`	°C	Second knot in initial temperature profile set near the estimated depth of zero annual amplitude.
`T0@bottom`	°C	Bottom knot in initial temperature profile set at the lower gird boundary (1000 m below the surface).
`T0_depth`	m	Depth to permafrost base in initial temperature profile.
`[layer].por`	-	Natural porosity of soil material in the given `layer`.
`[layer].org`	-	Organic fraction of solid material in the given `layer`.
`[layer].sat`	-	Water/ice saturation index of the given `layer`.
`[layer].`α`.log`α	-	Log transformed van Genuchten α parameter.
`[layer].n.logn`	-	Log transformed van Genuchten n parameter.
`[layer].Tm`	°C	Melting point of ground ice.

Table S2: Parameter prior distributions for Samoylov Island simulations

parameter	**prior**	**mean**	**stdev**	**units**
`nfw@initial`	Beta(α=13.00, β=7.00)	0.65	0.10	-
`nfw@2000`	Beta(α=13.00, β=7.00)	0.65	0.10	-
`nfw@2005`	Beta(α=13.00, β=7.00)	0.65	0.10	-
`nfw@2010`	Beta(α=13.00, β=7.00)	0.65	0.10	-
`nfw@2015`	Beta(α=13.00, β=7.00)	0.65	0.10	-
`nfs@initial`	Beta(α=18.00, β=2.00)	0.90	0.07	-
`nfs@2000`	Beta(α=18.00, β=2.00)	0.90	0.07	-
`nfs@2005`	Beta(α=18.00, β=2.00)	0.90	0.07	-
`nfs@2010`	Beta(α=18.00, β=2.00)	0.90	0.07	-
`nfs@2015`	Beta(α=18.00, β=2.00)	0.90	0.07	-
`topsoil.por`	Beta(α=40.00, β=10.00)	0.80	0.06	-
`topsoil.org`	Beta(α=37.50, β=12.50)	0.75	0.06	-
`topsoil.Tm`	Truncated(Normal(μ=0.00, σ=0.50); lower=-10.00, upper=0.00)	-0.40	0.30	°C
`topsoil.`α`.log`α	Normal(μ=-2.88, σ=0.17)	-2.88	0.17	-
`topsoil.n.logn`	Normal(μ=0.64, σ=0.18)	0.64	0.18	-
`sediment1.por`	Beta(α=40.00, β=10.00)	0.80	0.06	-

parameter	prior	mean	stdev	units
sediment1.Tm	Truncated(Normal(μ=0.00, σ=0.50); lower=-10.00, upper=0.00)	-0.40	0.30	°C
sediment1.α.logα	Normal(μ=-2.88, σ=0.17)	-2.88	0.17	-
sediment1.n.logn	Normal(μ=0.64, σ=0.18)	0.64	0.18	-
sediment2.xic	Beta(α=15.00, β=35.00)	0.30	0.06	-
sediment2.por	Beta(α=27.50, β=22.50)	0.55	0.07	-
sediment2.Tm	Truncated(Normal(μ=0.00, σ=0.50); lower=-10.00, upper=0.00)	-0.40	0.30	°C
sediment2.α.logα	Normal(μ=-2.88, σ=0.17)	-2.88	0.17	-
sediment2.n.logn	Normal(μ=0.64, σ=0.18)	0.64	0.18	-
sediment3.por	Beta(α=25.00, β=25.00)	0.50	0.07	-
sediment3.Tm	Truncated(Normal(μ=0.00, σ=0.50); lower=-10.00, upper=0.00)	-0.40	0.30	°C
sediment3.α.logα	Normal(μ=-2.88, σ=0.17)	-2.88	0.17	-
sediment3.n.logn	Normal(μ=0.64, σ=0.18)	0.64	0.18	-
sediment4.por	Beta(α=15.00, β=35.00)	0.30	0.06	-
sediment4.Tm	Truncated(Normal(μ=0.00, σ=0.50); lower=-10.00, upper=0.00)	-0.40	0.30	°C
sediment4.α.logα	Normal(μ=-2.88, σ=0.17)	-2.88	0.17	-
sediment4.n.logn	Normal(μ=0.64, σ=0.18)	0.64	0.18	-
T0@active_layer	Normal(μ=-5.00, σ=1.00)	-5.00	1.00	°C
T0@zaa	Normal(μ=-12.00, σ=3.00)	-12.00	3.00	°C
T0_depth	Truncated(Normal(μ=500.00, σ=100.00); lower=100.00, upper=900.00)	500.00	99.95	m
T0@bottom	Normal(μ=-12.00, σ=5.00)	-12.00	5.00	°C

Table S3: Parameter prior distributions for Bayelva simulations

parameter	prior	mean	stdev	units
nfw@initial	Beta(α=8.00, β=12.00)	0.40	0.11	-
nfw@2000	Beta(α=8.00, β=12.00)	0.40	0.11	-
nfw@2005	Beta(α=8.00, β=12.00)	0.40	0.11	-
nfw@2010	Beta(α=8.00, β=12.00)	0.40	0.11	-
nfw@2015	Beta(α=8.00, β=12.00)	0.40	0.11	-
nfs@initial	Beta(α=18.00, β=2.00)	0.90	0.07	-
nfs@2000	Beta(α=18.00, β=2.00)	0.90	0.07	-
nfs@2005	Beta(α=18.00, β=2.00)	0.90	0.07	-
nfs@2010	Beta(α=18.00, β=2.00)	0.90	0.07	-
nfs@2015	Beta(α=18.00, β=2.00)	0.90	0.07	-
topsoil.por	Beta(α=22.50, β=27.50)	0.45	0.07	-
topsoil.sat	Beta(α=60.00, β=40.00)	0.60	0.05	-
topsoil.org	Beta(α=2.50, β=47.50)	0.05	0.03	-
topsoil.Tm	Truncated(Normal(μ=0.00, σ=0.50); lower=-10.00, upper=0.00)	-0.40	0.30	°C
topsoil.α.logα	Normal(μ=-1.24, σ=0.23)	-1.24	0.23	-
topsoil.n.logn	Normal(μ=-1.01, σ=0.08)	-1.01	0.08	-
sediment1.por	Beta(α=25.00, β=25.00)	0.50	0.07	-
sediment1.sat	Beta(α=70.00, β=30.00)	0.70	0.05	-
sediment1.Tm	Truncated(Normal(μ=0.00, σ=0.50); lower=-10.00, upper=0.00)	-0.40	0.30	°C
sediment1.α.logα	Normal(μ=-1.76, σ=0.19)	-1.76	0.19	-

parameter	prior	mean	stdev	units
sediment1.n.logn	Normal(μ=-1.22, σ=0.04)	-1.22	0.04	-
sediment2.por	Beta(α=25.00, β=25.00)	0.50	0.07	-
sediment2.sat	Beta(α=80.00, β=20.00)	0.80	0.04	-
sediment2.Tm	Truncated(Normal(μ=0.00, σ=0.50); lower=-10.00, upper=0.00)	-0.40	0.30	°C
sediment2.α.logα	Normal(μ=-2.23, σ=0.06)	-2.23	0.06	-
sediment2.n.logn	Normal(μ=-1.10, σ=0.02)	-1.10	0.02	-
sediment3.por	Beta(α=20.00, β=30.00)	0.40	0.07	-
sediment3.Tm	Truncated(Normal(μ=0.00, σ=0.50); lower=-10.00, upper=0.00)	-0.40	0.30	°C
sediment3.α.logα	Normal(μ=-1.24, σ=0.23)	-1.24	0.23	-
sediment3.n.logn	Normal(μ=-1.01, σ=0.08)	-1.01	0.08	-
sediment4.por	Beta(α=15.00, β=35.00)	0.30	0.06	-
sediment4.Tm	Truncated(Normal(μ=0.00, σ=0.50); lower=-10.00, upper=0.00)	-0.40	0.30	°C
sediment4.α.logα	Normal(μ=-1.24, σ=0.23)	-1.24	0.23	-
sediment4.n.logn	Normal(μ=-1.01, σ=0.08)	-1.01	0.08	-
T0@active_layer	Normal(μ=-3.00, σ=1.00)	-3.00	1.00	°C
T0@zaa	Normal(μ=-5.00, σ=2.00)	-5.00	2.00	°C
T0_depth	Truncated(Normal(μ=500.00, σ=100.00); lower=100.00, upper=900.00)	500.00	99.95	m
T0@bottom	Normal(μ=10.20, σ=5.00)	10.20	5.00	°C

Table S4: Parameter prior distributions for Barrow simulations

parameter	prior	mean	stdev	units
nfw@initial	Beta(α=13.00, β=7.00)	0.65	0.10	-
nfw@2000	Beta(α=13.00, β=7.00)	0.65	0.10	-
nfw@2005	Beta(α=13.00, β=7.00)	0.65	0.10	-
nfw@2010	Beta(α=13.00, β=7.00)	0.65	0.10	-
nfw@2015	Beta(α=13.00, β=7.00)	0.65	0.10	-
nfs@initial	Beta(α=18.00, β=2.00)	0.90	0.07	-
nfs@2000	Beta(α=18.00, β=2.00)	0.90	0.07	-
nfs@2005	Beta(α=18.00, β=2.00)	0.90	0.07	-
nfs@2010	Beta(α=18.00, β=2.00)	0.90	0.07	-
nfs@2015	Beta(α=18.00, β=2.00)	0.90	0.07	-
topsoil.por	Beta(α=32.50, β=17.50)	0.65	0.07	-
topsoil.sat	Beta(α=80.00, β=20.00)	0.80	0.04	-
topsoil.org	Beta(α=25.00, β=25.00)	0.50	0.07	-
topsoil.Tm	Truncated(Normal(μ=0.00, σ=0.50); lower=-10.00, upper=0.00)	-0.40	0.30	°C
topsoil.α.logα	Normal(μ=-1.76, σ=0.19)	-1.76	0.19	-
topsoil.n.logn	Normal(μ=-1.22, σ=0.04)	-1.22	0.04	-
sediment1.por	Beta(α=27.50, β=22.50)	0.55	0.07	-
sediment1.sat	Beta(α=90.00, β=10.00)	0.90	0.03	-
sediment1.Tm	Truncated(Normal(μ=0.00, σ=0.50); lower=-10.00, upper=0.00)	-0.40	0.30	°C
sediment1.α.logα	Normal(μ=-1.76, σ=0.19)	-1.76	0.19	-
sediment1.n.logn	Normal(μ=-1.22, σ=0.04)	-1.22	0.04	-
sediment2.xic	Beta(α=15.00, β=35.00)	0.30	0.06	-

parameter	prior	mean	stdev	units
sediment2.por	Beta(α=27.50, β=22.50)	0.55	0.07	-
sediment2.Tm	Truncated(Normal(μ=0.00, σ=0.50); lower=-10.00, upper=0.00)	-0.40	0.30	°C
sediment2.α.logα	Normal(μ=-1.76, σ=0.19)	-1.76	0.19	-
sediment2.n.logn	Normal(μ=-1.22, σ=0.04)	-1.22	0.04	-
sediment3.por	Beta(α=27.50, β=22.50)	0.55	0.07	-
sediment3.Tm	Truncated(Normal(μ=0.00, σ=0.50); lower=-10.00, upper=0.00)	-0.40	0.30	°C
sediment3.α.logα	Normal(μ=-1.76, σ=0.19)	-1.76	0.19	-
sediment3.n.logn	Normal(μ=-1.22, σ=0.04)	-1.22	0.04	-
sediment4.por	Beta(α=22.50, β=27.50)	0.45	0.07	-
sediment4.Tm	Truncated(Normal(μ=0.00, σ=0.50); lower=-10.00, upper=0.00)	-0.40	0.30	°C
sediment4.α.logα	Normal(μ=-1.76, σ=0.19)	-1.76	0.19	-
sediment4.n.logn	Normal(μ=-1.22, σ=0.04)	-1.22	0.04	-
T0@active_layer	Normal(μ=-5.00, σ=1.00)	-5.00	1.00	°C
T0@zaa	Normal(μ=-9.10, σ=3.00)	-9.10	3.00	°C
T0_depth	Truncated(Normal(μ=500.00, σ=100.00); lower=100.00, upper=900.00)	500.00	99.95	m
T0@bottom	Normal(μ=10.20, σ=5.00)	10.20	5.00	°C

Table S5: Parameter prior distributions for Parson's Lake simulations

parameter	prior	mean	stdev	units
nfw@initial	Beta(α=10.00, β=10.00)	0.50	0.11	-
nfw@2000	Beta(α=10.00, β=10.00)	0.50	0.11	-
nfw@2005	Beta(α=10.00, β=10.00)	0.50	0.11	-
nfw@2010	Beta(α=10.00, β=10.00)	0.50	0.11	-
nfw@2015	Beta(α=10.00, β=10.00)	0.50	0.11	-
nfs@initial	Beta(α=18.00, β=2.00)	0.90	0.07	-
nfs@2000	Beta(α=18.00, β=2.00)	0.90	0.07	-
nfs@2005	Beta(α=18.00, β=2.00)	0.90	0.07	-
nfs@2010	Beta(α=18.00, β=2.00)	0.90	0.07	-
nfs@2015	Beta(α=18.00, β=2.00)	0.90	0.07	-
topsoil.por	Beta(α=30.00, β=20.00)	0.60	0.07	-
topsoil.sat	Beta(α=70.00, β=30.00)	0.70	0.05	-
topsoil.org	Beta(α=5.00, β=45.00)	0.10	0.04	-
topsoil.Tm	Truncated(Normal(μ=0.00, σ=0.50); lower=-10.00, upper=0.00)	-0.40	0.30	°C
topsoil.α.logα	Normal(μ=-2.88, σ=0.17)	-2.88	0.17	-
topsoil.n.logn	Normal(μ=0.64, σ=0.18)	0.64	0.18	-
sediment1.por	Beta(α=25.00, β=25.00)	0.50	0.07	-
sediment1.sat	Beta(α=80.00, β=20.00)	0.80	0.04	-
sediment1.Tm	Truncated(Normal(μ=0.00, σ=0.50); lower=-10.00, upper=0.00)	-0.40	0.30	°C
sediment1.α.logα	Normal(μ=-2.88, σ=0.17)	-2.88	0.17	-
sediment1.n.logn	Normal(μ=0.64, σ=0.18)	0.64	0.18	-
sediment2.xic	Beta(α=2.50, β=47.50)	0.05	0.03	-
sediment2.por	Beta(α=15.00, β=35.00)	0.30	0.06	-
sediment2.sat	Beta(α=90.00, β=10.00)	0.90	0.03	-

parameter	prior	mean	stdev	units
sediment2.Tm	Truncated(Normal(μ=0.00, σ=0.50); lower=-10.00, upper=0.00)	-0.40	0.30	°C
sediment2.α.logα	Normal(μ=-2.23, σ=0.06)	-2.23	0.06	-
sediment2.n.logn	Normal(μ=-1.10, σ=0.02)	-1.10	0.02	-
sediment3.xic	Beta(α=12.50, β=37.50)	0.25	0.06	-
sediment3.por	Beta(α=20.00, β=30.00)	0.40	0.07	-
sediment3.Tm	Truncated(Normal(μ=0.00, σ=0.50); lower=-10.00, upper=0.00)	-0.40	0.30	°C
sediment3.α.logα	Normal(μ=-2.88, σ=0.17)	-2.88	0.17	-
sediment3.n.logn	Normal(μ=0.64, σ=0.18)	0.64	0.18	-
sediment4.por	Beta(α=15.00, β=35.00)	0.30	0.06	-
sediment4.Tm	Truncated(Normal(μ=0.00, σ=0.50); lower=-10.00, upper=0.00)	-0.40	0.30	°C
sediment4.α.logα	Normal(μ=-1.76, σ=0.19)	-1.76	0.19	-
sediment4.n.logn	Normal(μ=-1.22, σ=0.04)	-1.22	0.04	-
T0@active_layer	Normal(μ=-7.00, σ=1.00)	-7.00	1.00	°C
T0@zaa	Normal(μ=-5.10, σ=2.00)	-5.10	2.00	°C
T0_depth	Truncated(Normal(μ=500.00, σ=100.00); lower=100.00, upper=900.00)	500.00	99.95	m
T0@bottom	Normal(μ=10.20, σ=5.00)	10.20	5.00	°C

S2.2 Parameter sensitivity analysis

The Bayesian ensemble inversion procedure described in the main text provides estimates of the most likely parameter values given the available ground temperature measurements by approximating samples from the posterior distribution. The posterior does not, however, directly provide a clear picture of which parameters are most influential with respect to specific model outputs. This influence can be quantified through parameter sensitivity analyses which attempt to determine the contribution of individual parameters to a particular scalar output quantity of interest (Saltelli, 2008).

The gold standard of such sensitivity analyses is generally thought to be the Sobol' indices (Sobol′, 2001) which are derived from the decomposition of an arbitrary, k-dimensional, square-integrable function f into additive components:

$$f = f_0 + \sum_i f_i + \sum_i \sum_{i>1} f_{ij} + \cdots + f_{1,2,\ldots,k} \tag{2}$$

where $f_i = f_i(X_i)$, $f_{ij} = f_{ij}(X_{ij})$, et cetera. The first-order contribution of the i'th parameter to the overall variance of $Y = f(\mathbf{X})$ can be quantified as:

$$S_i = \frac{\mathrm{Var}[\mathbb{E}[Y|X_i]]}{\mathrm{Var}[Y]} \tag{3}$$

Practical computation of these indices is, however, non-trivial. Typically tens of thousands of simulations following a specialized sampling procedure are required in order to obtain robust estimates (Saltelli, 2008).

We applied the Effective Algorithm for the computation of global Sensitivity Indices (EASI) of Plischke (2010) as implemented by Dixit and Rackauckas (2022) to the results of our ensemble simulations. We used EASI specifically due to its efficiency in being able to compute the first-order Sobol′ indices S_i without additional simulations. We included only parameter sample/output pairs from the first EKS iteration (i.e. the samples from the prior) to avoid the issue of correlations arising in the posterior samples which can affect the calculated sensitivities (Li et al., 2010). Note that, as a result, our sample size is relatively small ($N = 512$) which limits to some extent the reliability of the estimated sensitivity indices due to sampling effects (see Fig. 4 of Plischke (2010) for a sample size analysis). The results of this analysis are shown in Figs. S1-S4.

The results of this analysis indicate very clearly that the model outputs are most sensitive to the initial and boundary condition parameters which is also consistent with previous findings in other modeling studies (Garnello et al., 2021; Harp et al., 2016).

However, the latent heat trend is generally also sensitive to the porosity and excess ice content of the largest stratigraphy layers which of course determine the amount of water mass present in the system and thus consquently also the amount of latent heat that can be stored in these layers. We note also that the upper soil layers typically have minimal impact on all four output quantities considered; this is, however, likely a product of our modeling setup since we generally only consider annually averaged quantities which largely ignores the intraannual variability of the active layer.

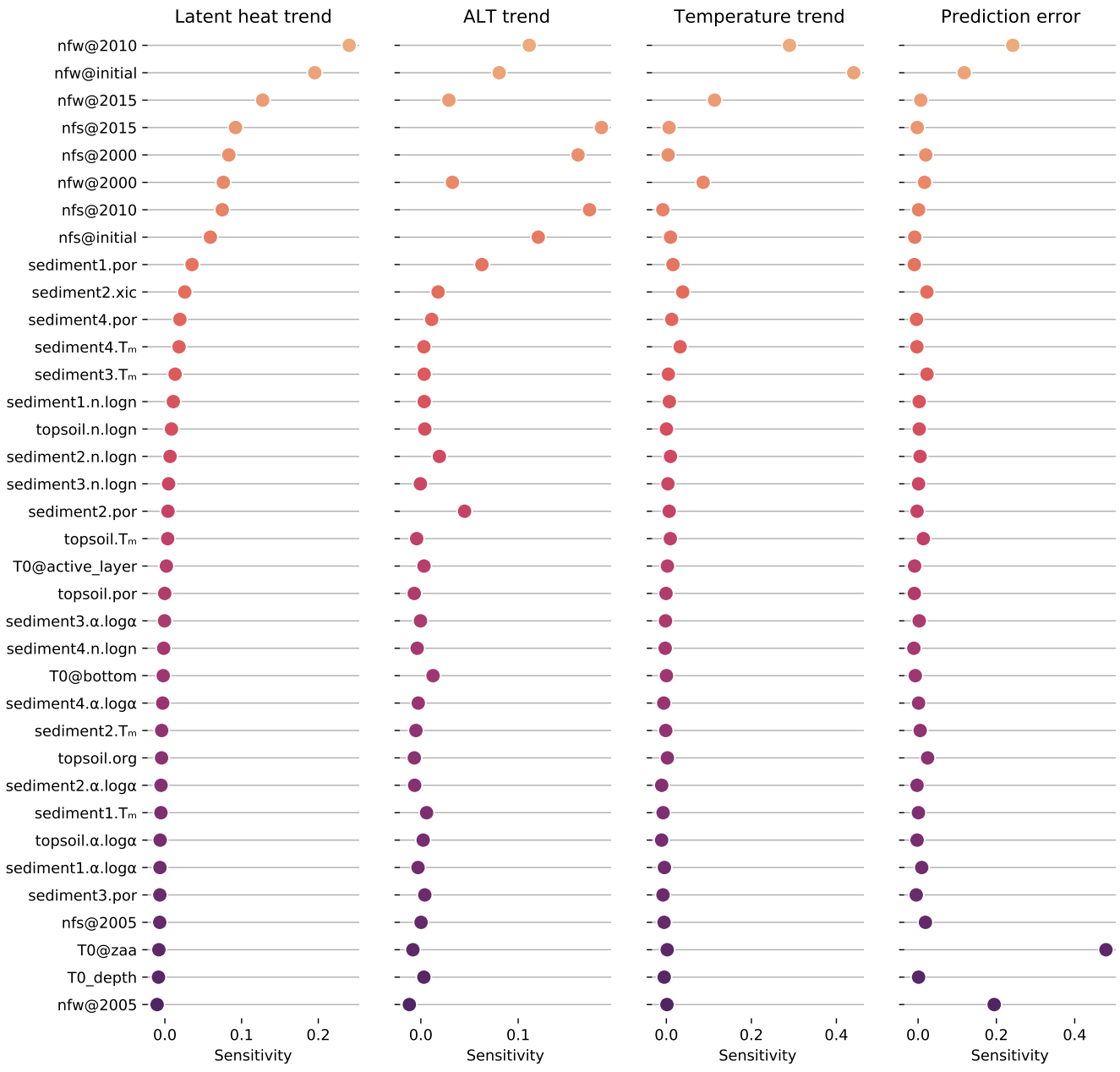

Figure S6. Samoylov Island model parameter sensitivities (first order Sobol′ indices) w.r.t to the latent heat trend, active layer thickness (ALT) trend, temperature trend, and ground temperature prediction error estimated with the EASI algorithm

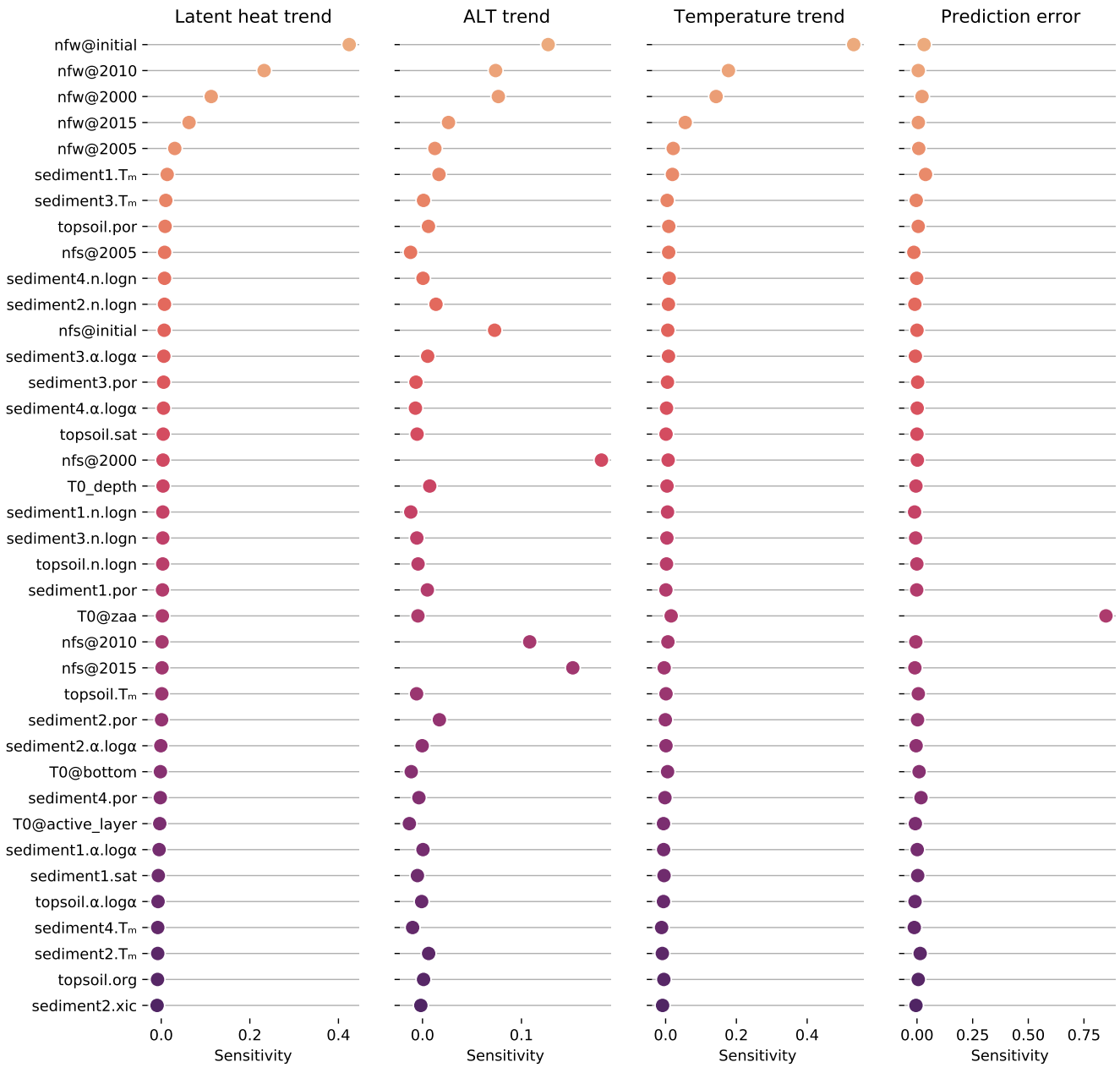

Figure S7. Barrow model parameter sensitivities (first order Sobol′ indices) w.r.t to the latent heat trend, active layer thickness (ALT) trend, temperature trend, and ground temperature prediction error estimated with the EASI algorithm

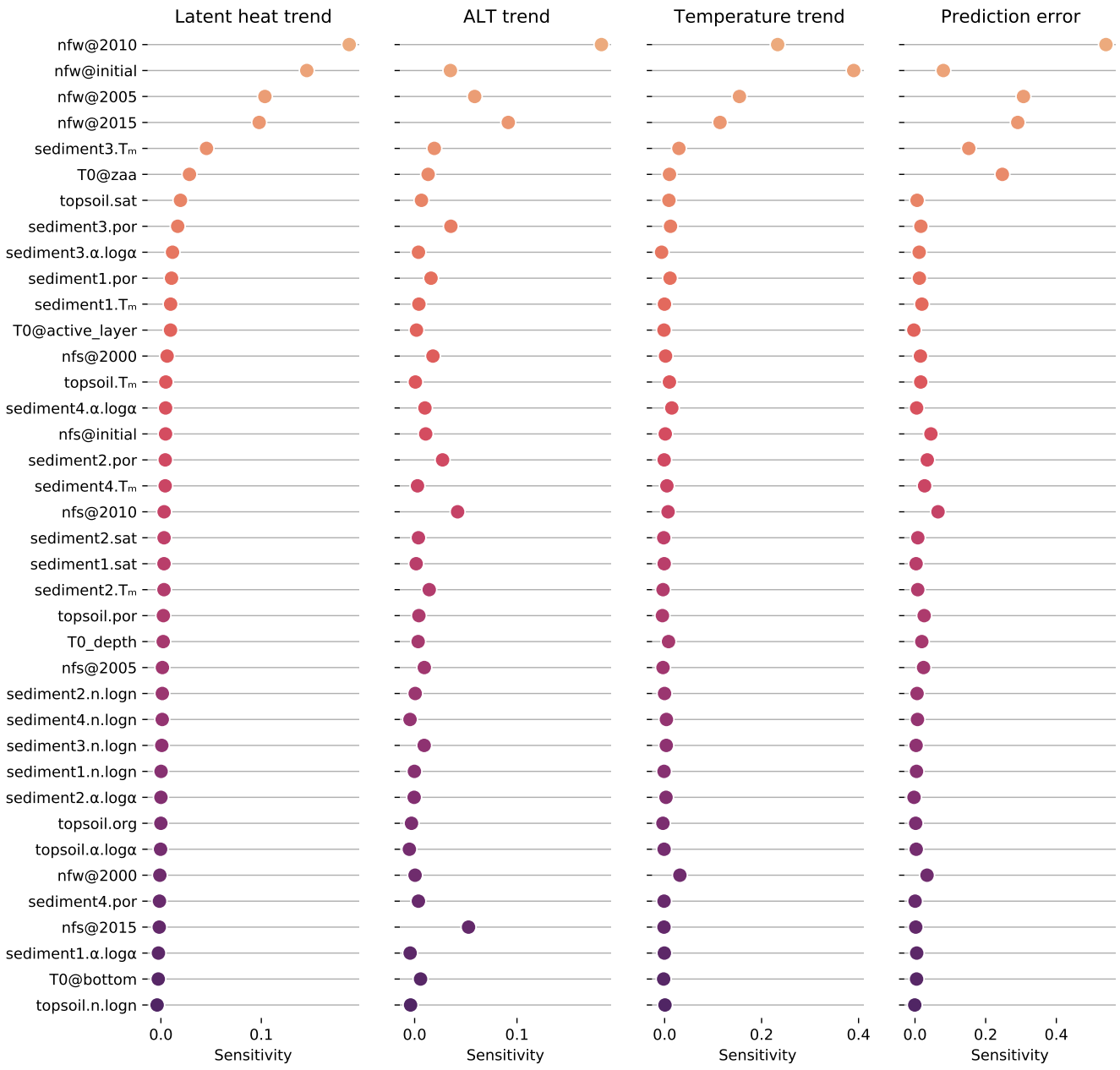

Figure S8. Bayelva model parameter sensitivities (first order Sobol′ indices) w.r.t to the latent heat trend, active layer thickness (ALT) trend, temperature trend, and ground temperature prediction error estimated with the EASI algorithm

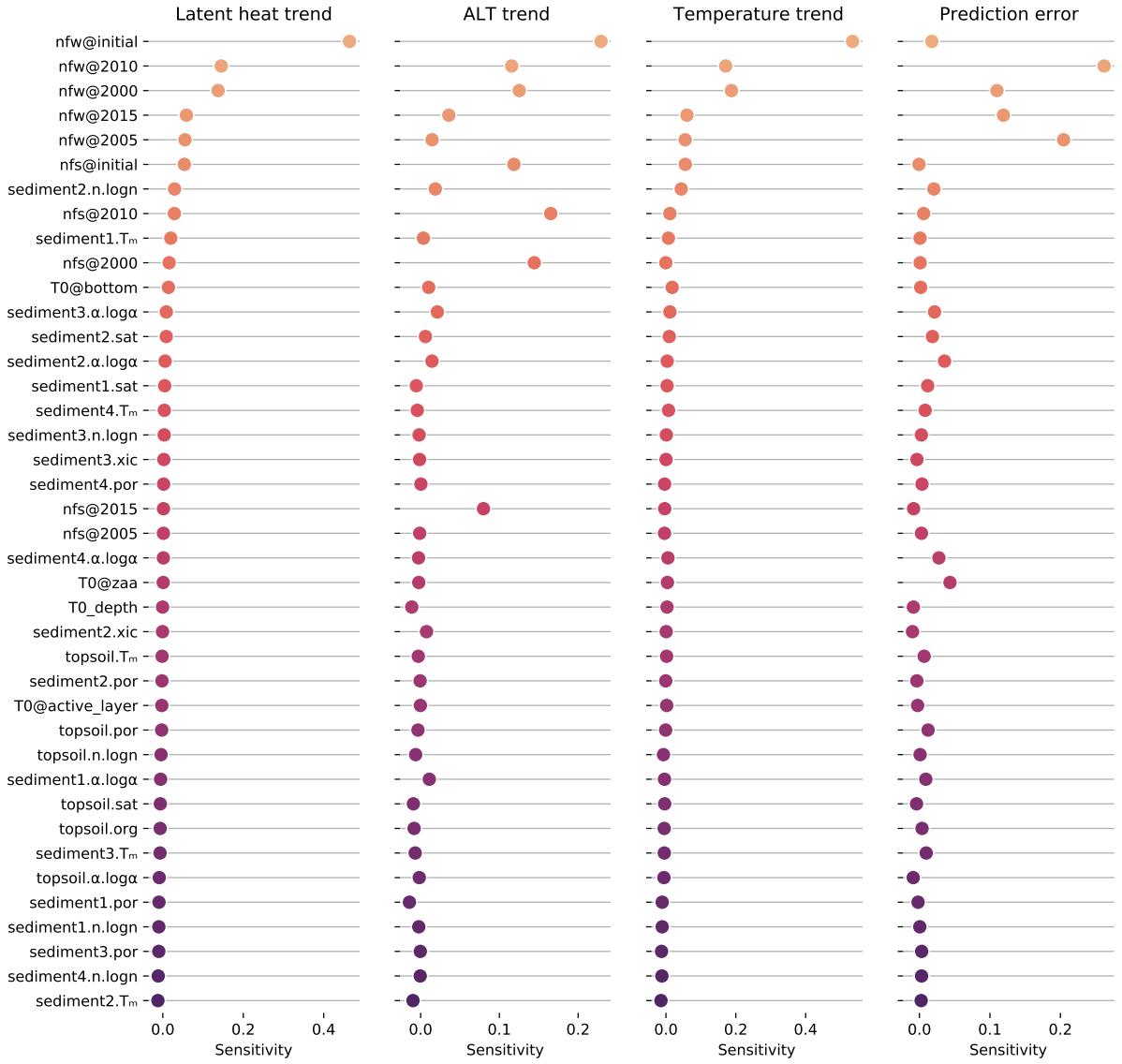

Figure S9. Parson's Lake model parameter sensitivities (first order Sobol′ indices) w.r.t to the latent heat trend, active layer thickness (ALT) trend, temperature trend, and ground temperature prediction error estimated with the EASI algorithm

References

Boike, J., Nitzbon, J., Anders, K., Grigoriev, M., Bolshiyanov, D., Langer, M., Lange, S., Bornemann, N., Morgenstern, A., Schreiber, P., Wille, C., Chadburn, S., Gouttevin, I., Burke, E., and Kutzbach, L.: A 16-Year Record (2002–2017) of Permafrost, Active-Layer, and Meteorological Conditions at the Samoylov Island Arctic Permafrost Research Site, Lena River Delta, Northern Siberia: An Opportunity to Validate Remote-Sensing Data and Land Surface, Snow, and Permafrost Models, Earth System Science Data, 11, 261–299, https://doi.org/10.5194/essd-11-261-2019, 2019.

Dixit, V. K. and Rackauckas, C.: GlobalSensitivity. Jl: Performant and Parallel Global Sensitivity Analysis with Julia, Journal of Open Source Software, 7, 4561, 2022.

Garnello, A., Marchenko, S., Nicolsky, D., Romanovsky, V., Ledman, J., Celis, G., Schädel, C., Luo, Y., and Schuur, E. a. G.: Projecting Permafrost Thaw of Sub-Arctic Tundra With a Thermodynamic Model Calibrated to Site Measurements, Journal of Geophysical Research: Biogeosciences, 126, e2020JG006 218, https://doi.org/10.1029/2020JG006218, 2021.

Harp, D. R., Atchley, A. L., Painter, S. L., Coon, E. T., Wilson, C. J., Romanovsky, V. E., and Rowland, J. C.: Effect of Soil Property Uncertainties on Permafrost Thaw Projections: A Calibration-Constrained Analysis, The Cryosphere, 10, 341–358, https://doi.org/10.5194/tc-10-341-2016, 2016.

Li, G., Rabitz, H., Yelvington, P. E., Oluwole, O. O., Bacon, F., Kolb, C. E., and Schoendorf, J.: Global Sensitivity Analysis for Systems with Independent and/or Correlated Inputs, The Journal of Physical Chemistry A, 114, 6022–6032, https://doi.org/10.1021/jp9096919, 2010.

Plischke, E.: An Effective Algorithm for Computing Global Sensitivity Indices (EASI), Reliability Engineering & System Safety, 95, 354–360, https://doi.org/10.1016/j.ress.2009.11.005, 2010.

Saltelli, A., ed.: Global Sensitivity Analysis: The Primer, John Wiley, Chichester, England ; Hoboken, NJ, 2008.

Sobol′, I. M.: Global Sensitivity Indices for Nonlinear Mathematical Models and Their Monte Carlo Estimates, Mathematics and Computers in Simulation, 55, 271–280, https://doi.org/10.1016/S0378-4754(00)00270-6, 2001.